Embedded Soft Inductive Sensors to Measure Arterial Expansion of Tubular Diameters in Vascular Phantoms

Torjus L. Steffensen, Marius Auflem, Håvard N. Vestad, *Member, IEEE*, and Martin Steinert

***Abstract*—Measuring diameter change in flexible tubular structures embedded in opaque material is challenging. In this article, we present a soft braided coil embedded in an elastomer tube as a method to continuously measure such a change in diameter. By measuring the inductance change in the braided coil, we estimate the instantaneous diameter with a simple inductance model. In applying this method, we demonstrate that diameter waves in a vascular phantom, a model of a radial artery embedded in a viscoelastic wrist structure, can be recorded continuously. Four sensors were made, and their ability to measure physiologically relevant simulated pulse waves was assessed. Several pressure pulse profiles were generated using a precision digital pump. Inductance of the coil was measured simultaneously as the change in diameter was recorded using an optical laser/mirror deflection measurement. One sensor was then embedded in a vascular phantom model of the human wrist. The diameter of the simulated radial artery was recorded via ultrasound and estimated from coil inductance measurements. The diameter estimates from the inductance model corresponded well with the comparator in both experimental setups. We demonstrate that our method is a viable alternative to ultrasound in recording diameter waves in artery models. This opens opportunities in empirical investigations of physiologically interesting fluid-structure interaction. This method can provide new ability to measure diameter changes in tubular systems where access is obstructed.**

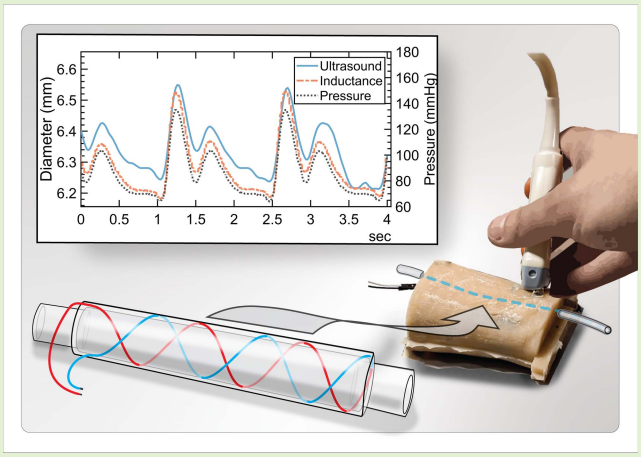

***Index Terms*—In vitro experimentation, inductance, soft electronics, measurement methods.**

I. Introduction

MEASURING pressure propagation in soft tubular structures is of interest in the field of arterial mechanics, where pulse wave propagation can be studied to make conclusions about arterial function [1]–[3]. Many tissues including arteries are viscoelastic [4], making accurate mathematical modeling challenging. Therefore, empirical in vitro experiments are frequently employed [5], [6]. The relationship between fluid forces acting on the wall structure and the resulting change in geometry from the induced strains is one topic of interest. The propagation of the strain energy through the vessel wall can be visualized as waves of expanding and contracting vessel diameter. In vitro models are often considered as freely suspended tubes, for sake of simplicity and observation. However, in cases where the interaction between the model vessel and the surrounding tissue is of interest, this is not feasible. In the case of radial tonometry, a technology that is seeing interest for applications in wearable blood pressure monitoring [7]–[9], the interaction between the vessel wall, the underlying bone, and the tissue between the vessel and skin surface are all important. This can be achieved by placing the vessel model inside tissue-mimicking material, obstructing view of the tube [10].

There are few methods to continuously measure a varying diameter in a soft tube inside an opaque material. Here, we propose a soft braided coil cast inside an elastomer tube wall as such a method. To allow for radial expansion from pressurizing the tube, the sensor consists of a high pitch helical coil. The coil is routed back and forth over the length of the tube section, resulting in a weaved braid pattern, as opposed to a sequentially stacked coil (Fig. 1).

A change in the tube's diameter also changes the diameter of the coil, which in turn alters its inductance. This principle has previously been applied in sensing actuation lengths in

Manuscript received January 22, 2022; revised February 23, 2022; accepted February 23, 2022. Date of publication February 25, 2022; date of current version March 31, 2022. The work of Marius Auflem was supported by the Research Council of Norway under Grant 290404. The associate editor coordinating the review of this article and approving it for publication was Dr. Edward Sazonov. *(Corresponding author: Torjus L. Steffensen.)*

Torjus L. Steffensen is with the Department of Circulation and Medical Imaging, Norwegian University of Science and Technology, 7025 Trondheim, Norway (e-mail: torjus.l.steffensen@ ntnu.no).

Marius Auflem, Håvard N. Vestad, and Martin Steinert are with the Department of Mechanical and Industrial Engineering, Norwegian University of Science and Technology, 7025 Trondheim, Norway.

Digital Object Identifier 10.1109/JSEN.2022.3155071

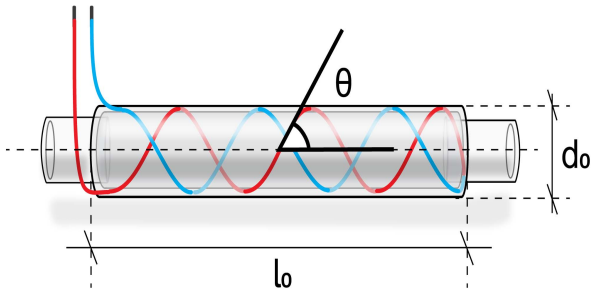

Fig. 1. Geometry of the sensor tube, showing the braided coil structure and connecting pressure tubes.

pneumatic actuators (McKibben muscles) [11], [12]. Similar flexible coils have also been used to determine angular change from the induced current resulting from the change in magnetic field caused by bending the coil [13]. Here, we focus on small, sub-millimeter changes in diameter caused by differences in internal pressure.

A. Detection Principle

With a fixed wire length, a braid pattern causes axial contraction of the helical structure from altered braid angles as the diameter increases. As the wire is routed in the same rotational direction around the tube the electromagnetic properties of the solenoid and current direction are preserved. We can then estimate the relationship between the cross-sectional area of the coil and the inductance L as in a long solenoid [11]:

$$L = \frac{\mu N^2 A}{l} \tag{1}$$

where N is the number of effective coil windings, μ is the magnetic permeability of the core (for air, we set μ approximately equal to vacuum permeability μ_0), and A is the cross-sectional area of the "solenoid". For a winding angle of 20° the model is roughly linear to the full extent of expansion and compression as limited by the braid [11]. In this work we operate well within this range.

The accuracy of the long solenoid model in braided soft actuators has been compared to more sophisticated inductance models [11], and while accuracy decreases with deformation size, for small deformations the error is small.

For a braided tube of length l, relaxed diameter D_0 and wire winding angle θ with respect to the long axis of the braid, assuming constant coil length and a circular cross section the length of the coil helix b is given by

$$b = \frac{l_e}{\cos(\theta)} \tag{2}$$

where l_e is the length of the fully relaxed tube. The number of turns each helix of the braid makes around the axis of the cylinder n is given by:

$$n = \frac{b \sin(\theta_0)}{\pi D_0} \tag{3}$$

TABLE I
TUBE DIMENSIONS

Tube no.	D_0	l_e	θ_0
1	6.2 mm	90 mm	25°
2	6.8 mm	58 mm	23°
3	5.3 mm	100 mm	18°
4	7.2 mm	75 mm	25°

Equation (3) along with the number of helices in the sensor gives us a value for the effective number of coil windings N [11], [14]. To determine a change in tube radius r from an associated change in inductance, we expand (1):

$$\Delta L = (L - L_0) = \frac{\mu N^2 \pi (r^2 - r_0^2)}{l} \tag{4}$$

Which is equivalent to:

$$r = \sqrt{\frac{(L - L_0) l}{\mu N^2 \pi} + r_0^2} \tag{5}$$

In a material with a positive Poisson's ratio the change in diameter necessarily also results in a contraction along the length of the tube. In the case of small deformations in a long thin tube, where $l \gg D$, we assume that the change in cylinder length is negligible in relation to the change in diameter and treat l as constant. The resulting relationship is nonlinear, but locally behaves approximately linearly for small deformations [12].

B. Sensor Fabrication

We made sensors by winding flexible silicone shielded wire onto a dowel. The resulting braids were then molded in Ecoflex 00-10 (Smooth-On, USA) by pouring and continuous rotation. Ecoflex 00-10 is a very soft elastomer, with a reported static Young's modulus of 0.05 MPa at 10% strain [15]. Removing the dowel, the resulting structure is a braided flexible wire embedded in a silicone tube of roughly uniform thickness.

We made four sensors to compare their behavior and to account for differences in coil characteristics due to the artisanal nature of the manufacturing process (Table I).

II. EXPERIMENTS & METHODS

A. Pressure Expansion

We conducted an experiment to assess the change in sensor induction due to expansion under pressure (Fig. 2). The sensor tube was fixed horizontally to an inclined plane, and the ends of the tube were fixed to prevent angular deformation during expansion and contraction.

The ends of the wire braids in the tube sensor were connected to a parallel capacitor, forming an LC oscillator circuit. This circuit was connected to an induction-to-digital converter (LDC1612, Texas Instruments, Texas, USA). The LDC1612 operates by applying a drive current to an LC circuit

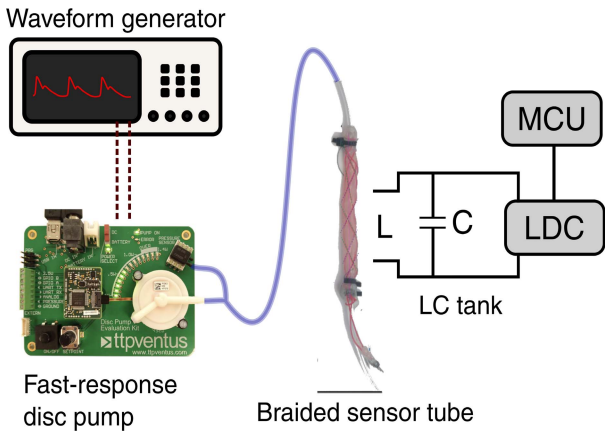

Fig. 2. Schematic illustration of the experimental setup.

and measuring the resulting primary oscillation frequency f_0. In our configuration the LDC was connected to an external 40 MHz reference oscillator, which is used to determine f_0. Given that the parallel capacitance C is known, this allows for the determination of the inductance L through the relationship

$$f_0 = \frac{1}{2\pi\sqrt{LC}} \tag{6}$$

Each of the four tubes was in turn connected to a precision digital control disc pump (XP-S2-028, TTP Ventus, UK). The other end of the tube was clamped shut, resulting in a controllable internal pressure when the pump was active. A differential pressure sensor (TSC 015PD, Honeywell International, USA) gauged the air pressure inside the tube against ambient atmosphere.

As the diameter of the tube changes in response to the pressure variation, as does the diameter of the coil, resulting in an increase in L. Thus f_0 varies over the course of the load cycle, allowing a calculation of L from (6).

The disc pump was controlled with an arbitrary waveform generator (UTG2025A, UNI-T, China). Inductance and pressure were recorded at three different load states (Table II). First, after setting up the experiment, one minute of inductance readings was recorded to establish L_0 for each tube in the unloaded state. Second, a 0.5 Hz square wave pressure cycle was applied to the tube for a period of 4 minutes. Pressure was then allowed to equalize to ambient pressure. Lastly an arterial pulse pressure waveform was applied for 1 minute. The wave profile was recorded from the proper palmar digital artery at the middle phalanx of the left middle finger using a volume-clamp apparatus (NIBP Nano INL382, ADInstruments, Dunedin, New Zealand).

Data was collected on a Windows PC and processed in MATLAB r2021a (The Mathworks, Massachusetts, USA).

B. Response Validation

To record the change in tube diameter, the tube was fixed to an angled plate and restricted in a single point with cyanoacrylate glue, allowing it to expand and retract with the center of the tube moving normally to the angled plate.

TABLE II
EXPERIMENTAL PROTOCOL

Load type	Cycle Frequency	Pressure range	Duration
Zero load	n/a	Ambient	1 minute
Square wave	0.5 Hz	30 - 90 mmHg	4 minutes
Arterial wave	1 Hz	40 – 100 mmHg	1 minute

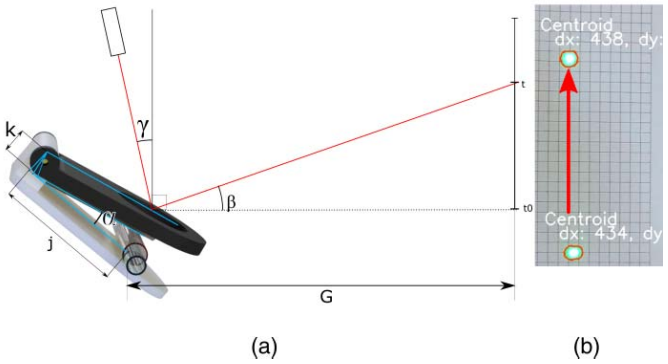

Fig. 3. (a) Schematic of laser measurement geometry used to measure expansion and contraction of the tubes. (b) Illustration of the laser dot tracking. Not to scale.

A mirror, rotating freely on a hinge, was placed resting on top of the tube. The expansion of the tube then resulted in a small angular change of the mirror, proportional to the increase in diameter of the tube (Fig. 3). A laser was focused on the mirror at an angle, and the resulting laser dot was recorded moving against a reference scale placed at a distance to amplify the movement [16].

The diameter of the tube could then be determined from the motion of the laser dot through a trigonometric relationship:

$$r \cong \tan\left(\frac{\tan^{-1}\left(\frac{t_1}{G}\right)+\gamma+2\alpha_0}{4}\right) \times\left(j+k\tan\left(\frac{\tan^{-1}\left(\frac{t_1}{G}\right)+\gamma+2\alpha_0}{4}\right)\right) \tag{7}$$

where r is the radius, t is the height of the laser dot on the target relative to the height of the mirror, k is the vertical distance from the hinge point to the baseplate where the tube is fixed (8.5mm), j is the lateral distance from hinge point to fixation point of tube (40mm), G is the horizontal distance between mirror and target (9980mm), and α_0 is the angle of the mirror hinge where the resulting angle between mirror and the horizontal plane is 45 degrees (7.5 degrees). γ is the angular deviation of the laser from the vertical axis. This is tuned with an adjustment screw on the laser to hit the target regardless of the different diameters of the tubes. γ is calculated using (7) and a caliper measurement of the diameter of the tube.

We recorded the movement of the laser dot with a digital camera at a resolution of 3840×2160 pixels. Frame to frame position was determined using open-source video analysis

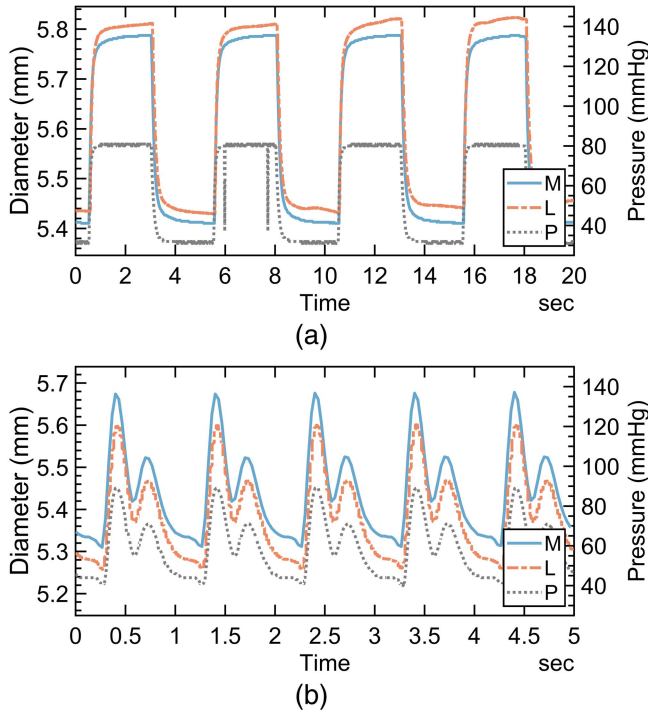

Fig. 4. Change in tube diameter from applied internal pressure, measured via mirror deflection, and estimated from inductance. M: diameter measured via mirror deflection, L: diameter estimate from inductance measurement, P: internal tube pressure. (a) 0.5 Hz square wave. (b) 1 Hz radial pulse wave.

tools (OpenCV) and referenced against the background scale. The result is a time series of the tube diameter with a time step resolution of 30 samples per second and a geometric resolution of 3.56 pixels per mm of laser movement (Fig. 4).

Equation (7) is simplified and does not account for vertical movement of the mirror. These effects result in a vertical displacement of the laser dot less than the total diameter change of the tube, which is negligible in comparison to the displacement of the dot due to angular change.

C. Drift Measurement

We observed significant sensor drift during long recordings. To assess the scale of drift in ambient conditions and the influence of temperature we placed a tube sensor on a vibration isolated table exposed to ambient atmosphere over 24 hours and applied a 0.5 Hz square-wave pressure load cycle. Inductance was measured from the coil alongside ambient temperature with a BMP388 atmospheric pressure and temperature sensor (Bosch Sensortec, Germany) in the immediate vicinity of the tube (Fig. 5). Drift was confirmed and appeared to behave approximately linearly in the first regime (zero to sixteen hours), before a temperature impulse caused a dramatic upwards spike. We believe this impulse to have been caused by the sun shining on our lab, a hypothesis supported by in situ meteorological observations.

For the first 7 hours, the temperature sensor reported rising temperatures with a seemingly logistic growth. A likely

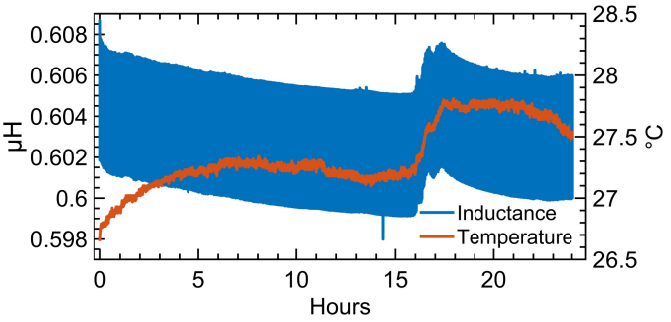

Fig. 5. Inductance recorded over a 24-hour 0.5 Hz load cycle in ambient conditions. Drift appears to behave linearly in the first 15 hours.

explanation is internal temperature increase in the temperature sensor itself once powered. In time the temperature sensor reaches equilibrium and disperses the same amount of heat as it produces to the surroundings, after which the temperature data seems to correspond well with the drift of the inductance sensor. Afterwards, the response of the inductance measurement to the temperature spike suggests the drift is dominated by thermal effects. This sensitivity to small changes in temperature must be considered in applications.

We performed a linear regression on the component of the drift occurring before the temperature impulse took place, resulting in a slope of -1.48×10^{-10} H/hour.

D. Application in a Radial Artery Phantom

To assess the usability of these sensors in a vascular phantom we embedded one of the previously tested braided tube sensors in a wrist model. The wrist was cast in silicone elastomer (Ecoflex, Smooth-On, USA) in a mold produced via fused filament fabrication (FFF). The mold was modeled from a high-resolution scan of the human wrist. We also placed an FFF-printed radius and ulna bone from the same anatomical model into the cast to provide internal structure. The embedded tube had an inner diameter of 3 mm, matching a realistic range for the human radial artery[17] (Fig. 6).

We pressurized the tube system as before, but this time flushed it with water instead of air to allow ultrasound imaging. The pump compressed a small amount of air in the upstream tubing, acting as a piston on the internal water reservoir. The water was mainly static, although the pressure difference in the air piston resulted in minor oscillatory back-and-forth flow. We did not expect exchanging water for air to have a significant effect on the inductance in the coil, as the magnetic permeability of water is similar to that of air [18].

We investigated the flushed and pressurized phantom under ultrasound (Vivid E95, GE Healthcare) to compare the change in diameter of the embedded tube to that estimated from the inductance. We applied the same arterial pulse pressure profile. Due to the surrounding tissue now resisting compression, we had to apply a higher pressure to see the same range of diameter motion. The load varied between 70 – 135 mmHg, as measured in the air piston. This corresponds well to a realistic blood pressure range [4].

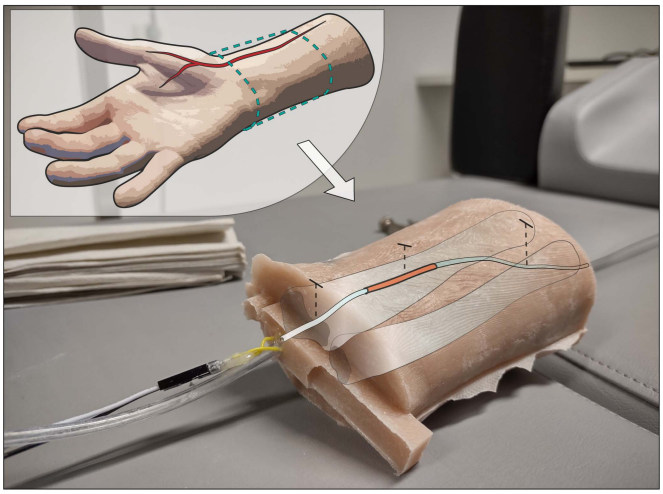

Fig. 6. Illustration of the wrist phantom with the placement of the radius, ulna, and sensor tube superimposed. The phantom simulates a section of the right wrist, with bone, blood vessel, and mediating tissue.

It is important to note that the material in the phantom has significantly different acoustic properties from those of human tissue. This difference must be accounted for when using equipment calibrated for real tissue. Most importantly for this application, the speed of sound differs, which will affect the calculated depth scale of the ultrasound machine. A rough compensation can be done by correcting for the difference in local speed of sound, also referred to as the propagation velocity:

$$z_{corr} = z\frac{C_{EF}}{C_T} \tag{8}$$

where z_{corr} is the corrected depth z, and C_t and C_{EF} are the propagation velocities in soft tissue and Ecoflex polymer respectively. As C varies between tissues, C_t is commonly taken to be the average value of several common types of soft tissue, approximately 1.54 m/s [19]. Together with the propagation velocity in the silicone material, 0.97 m/s [20], a correction factor of 0.63 is obtained. The propagation velocity in the phantom tissue is slower than the expected value for human tissue. The uncorrected depth therefore assumes a greater distance has been traveled by the reflected sound wave. If not corrected the estimated depth values will be erroneously large.

We measured the relaxed diameter a priori and confirmed this measurement under ultrasound B-mode to confirm good correspondence. In the M-mode configuration, a sequence of single ultrasound scan lines is collected and presented to illustrate the spatial movement of structures in the scan line over time. By recording the motion of the wall of the artery, a "diameter wave" can be obtained (Fig. 7). By combining the motion of a point in the tube wall with the initial, or smallest, diameter, the diameter of the vessel over time can be reconstructed. (Fig. 8) shows the diameter of the embedded soft tube determined in this way, alongside the diameter of the tube estimated using the same nominal starting diameter and the inductance measurement.

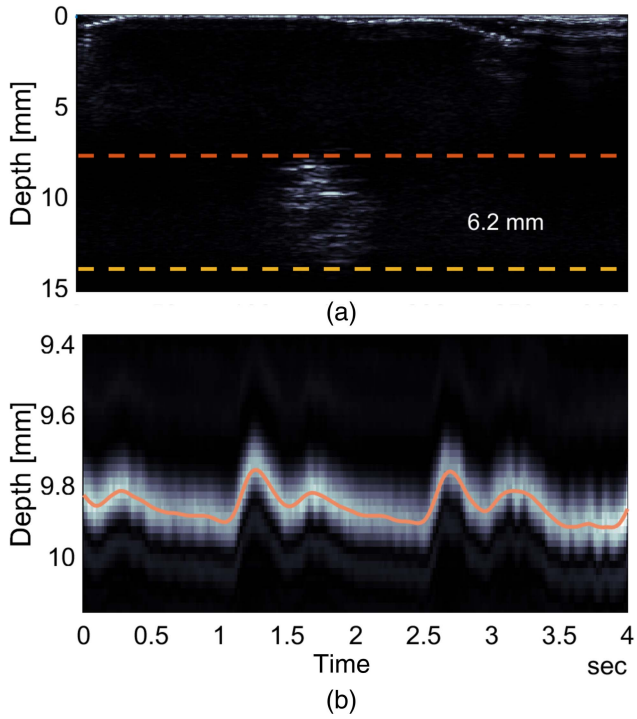

Fig. 7. (a) B-mode ultrasound of the wrist phantom, approximately 5 cm distal to the styloid process. Note that no effort was made to induce echogenicity in the phantom, resulting in a poorly defined image. (b) M-mode recording illustrating the pulsatile movement of the "lumen". A centerline trace of the tube wall has been superimposed.

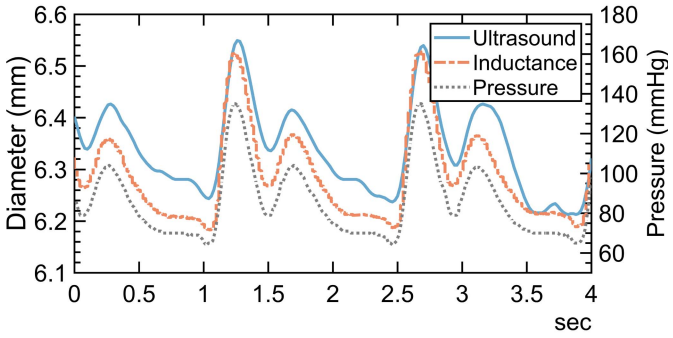

Fig. 8. Diameter calculated from phantom lumen wall movement from ultrasound plotted with the estimate from inductance. The profile of the pressure trace is consistent over the three cycles shown. At around 3 seconds a peak is shifted in the ultrasound trace. This is not reflected in the pressure or inductance curves, implying that it is an artifact introduced in the ultrasound recording.

III. Results and Discussion

Over the course of contraction and expansion, the sensor tube system experiences some hysteresis, as can be expected from the viscoelastic properties of the structural material (Fig. 9). Within the isolated loading and unloading regimes, a linear fit can still be made to estimate sensor sensitivity. Linear regression models were fitted on monotonically increasing tube expansion series using a robust fit method implemented in MATLAB's fitlm function. The results presented strong linear fits to the data (R^2 between 0.994 and 0.997). Apparent sensitivities corresponding to the regression

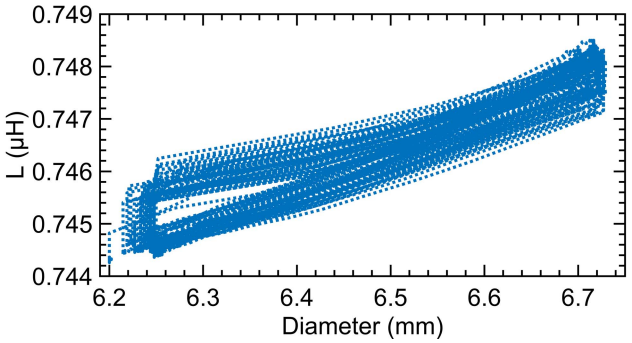

Fig. 9. Superposition of inductance and diameter traces measured over 4 minutes of cyclic loading, showing hysteresis as well as drift.

TABLE III
REGRESSION ESTIMATES OF BEST LINEAR FIT

Tube no.	Closest linear fit	Corresponding apparent sensitivity, 10^{-7} H/mm
1	$r = 6.58 \times 10^{-7} L - 46.08$	7.12
2	$r = 3.97 \times 10^{-7} L - 18.60$	4.89
3	$r = 4.96 \times 10^{-7} L - 20.15$	4.27
4	$r = 7.02 \times 10^{-7} L - 42.77$	6.20

model are presented in Table III. The sensitivity range agrees broadly with previous work [11]. The mean absolute error of the inductance estimate compared to the laser measurement ranged from 0.02 to 0.06 mm. This result is associated with some uncertainty, which is discussed later.

Sensor resolution in our setup is determined by the output of the LDC1612 converter, which has a total resolution of 28 bits. In practice, effective resolution is limited by the electromagnetic properties of the sensor element in the LC circuit and by the sample rate. As the LDC can essentially be viewed as a frequency-to-digital converter, the LSB is measured in Hz, and is determined primarily by the reference count of the converter and the variation of the signal frequency. We observed a typical frequency variation in our target signal of around 0.5%, which with a reference clock timed at 40 MHz and a sample rate of 300 Hz corresponds to 11 bits of effective resolution over the range of interest [21]. For the same configuration, reducing the sample rate to 100 Hz results in an increase in effective resolution to 12 bits as the reference count increases.

A. Error Sources

There are benefits and drawbacks to using LDCs compared to a benchtop LCR meter. Perhaps the clearest benefits are sampling rate, which can reach several thousand Hz under some circumstances, high portability, and low cost of implementation. But because the measured value of the LDC is the oscillation frequency of an LC circuit, it is necessary for the designer to have precise control of their coil characteristics. As tables I and III show, the sensitivity of the coil varies significantly with coil dimensions. As loosely wound, high-pitch coils such as the ones we have used here typically have small self-inductance values, the oscillation frequency is typically high without a very small parallel capacitance, as can be seen from (6). In our experiments, the sensor frequencies were between 6-8 MHz in this configuration. Lowering the parallel capacitance or adding inductors in series can bring the frequency range down, but this increases noise outside of the manufacturer's recommended capacitance range as the effects of parasitic capacitance in the coil become more noticeable [22] and reduces effective signal resolution. Skin effects also become significant at these frequency ranges, which may contribute some error to the estimates we derive from the inductance values. Skin effect is not accounted for in our model.

The parallel capacitor in our LC circuit was placed at the end of the connecting wires from the coil, rather than immediately outside the coil, which is the recommended configuration [21]. This may have contributed to a greater parasitic capacitance, resulting in an unstable source of error in the calculation of inductance from the oscillation frequency. In future applications the influence of the coil placement in relation to the measurement electronics should be considered.

Other sources of error relate to the uncertainty in our coil parameters. Much of this uncertainty is due to the hand-made nature of the coils. The winding angle, for example, may differ slightly over the length of the coil, as may the thickness of the polymer layer under the conductive material. The ends of the coil are also nonuniform because of the fabrication process. Improving this process so that coil geometry is more uniform would reduce this uncertainty in future applications.

Determining the diameter expansion of the tube using the laser and mirror setup is dependent on a geometric relationship which is subject to several simplifying assumptions and precision measurements. There is some uncertainty associated with the absolute values determined in this way. The pixel resolution of the laser measurement puts a lower bound on the absolute certainty of the measurement. The resolution of the video, at 0.278 mm per pixel, with an average of 255 pixels of laser travel corresponding to approximately 0.5 mm of expansion range results in a theoretical measurement resolution around 2 μm using the laser mirror setup. Errors due to simplifying assumptions in calculating the geometric relationship and imprecisions in the experimental setup are certainly larger than this resolution limit.

Significant drift was observed over the course of several-minute long recordings. The drift appeared to behave in a broadly linear manner, suggesting it could be compensated for. The sensitivity of the system to small changes in temperature poses some challenges to practical use. Temperature-sensitive elements in our experimental setup include the coil itself, the parallel capacitor, and the reference clock. The coil was not separated thermally from the measurement circuitry in our experiment, but as this more closely reflects the likely realities of a real-world application, the observed behavior may be more informative for the application designer. Perhaps most importantly, handling of the sensor might adversely affect the measurement. Regular calibration of the estimate value should be done against a known reference value.

B. Application Validation

Ultrasound recording over time is challenging. Even when recording structures that are relatively motionless, the probe must be kept perfectly still. Robot-assisted systems do exist, but are rare, and in most real cases ultrasound recordings will be done by hand [23]. The quality of the recording is therefore dependent on the skill of the operator. The practical consequence of this is that without skilled operators, many otherwise high-quality recordings may not be stable over time. In our data, the shape of the inductance measurement corresponds more closely to that of the internal pressure than the trace from the ultrasound, especially in the third cycle of the M-mode trace (Fig. 8). A likely explanation for this is instability of the ultrasound probe in relation to the "artery" over the time of the recording. In some situations, measurement of structural diameter from coil inductance could be a more reliable measure of internal geometry than operator-guided ultrasound in continuous recordings.

IV. Conclusion

We have presented the manufacture and application of soft sensor tubes consisting of braided wire coils wound inside a soft silicone rubber sleeve. As part of an LC tank together with an inductance-to-digital converter, these sensors can detect small changes in their diameter caused by differences in internal pressure with high fidelity. The sensor was sampled at 300 Hz and corresponded well with comparator measurements of the tube diameter collected optically and with ultrasound. The sample rate of the inductance measurement was higher than those easily achievable with the comparator methods, implying that the sensor might be useful in applications with high requirements for temporal resolution, such as pressure wave analysis.

While the sensor exhibits drift and hysteresis that could be prohibitive to very high precision measurements, presumably because of thermal and viscoelastic effects, the resolution was satisfactory for deformations in the tenths of a millimeter range. Linear drift seemed to be in correspondence to temperature changes in the ambient atmosphere, indicating that temperature compensation could be necessary in a practical application.

Soft braided coils embedded in flexible polymer can be used to estimate small deformations of embedded tubular structures using self-inductance, presenting an alternative to ultrasound in vascular phantoms. Possible applications include transient flow-through pressure impulse monitoring, pipe inspection, or mold channel cleaning.

In future work we want to recreate the results presented here using compliant conductors to avoid the composite effects of the coil structure on the mechanical properties of the tube. We intend to apply this well-performing measurement method to investigate numerical models of pressure coupling in the wrist for noninvasive wearable blood pressure sensors.

References

[1] D. Agnoletti *et al.*, "Pulse pressure amplification, pressure waveform calibration and clinical applications," *Atherosclerosis*, vol. 224, no. 1, pp. 108–112, Sep. 2012, doi: 10.1016/j.atherosclerosis.2012.06.055.

[2] M.-M. Laurila *et al.*, "Evaluation of printed P(VDF-TrFE) pressure sensor signal quality in arterial pulse wave measurement," *IEEE Sensors J.*, vol. 19, no. 23, pp. 11072–11080, Dec. 2019, doi: 10.1109/JSEN.2019.2934943.

[3] W. W. Nichols, M. F. O'Rourke, and C. Vlachopoulos, "Pressure pulse waveform analysis," in *McDonald's Blood Flow in Arteries. Theoretical, Experimental and Clinical Principles*, 6th ed. London, U.K.: Hodder Arnold, 2011.

[4] W. W. Nichols, M. F. O'Rourke, and C. Vlachopoulos, *McDonald's Blood Flow in Arteries. Theoretical, Experimental and Clinical Principles*, 6th ed. London, U.K.: Hodder Arnold, 2011.

[5] Y. Ma, J. Choi, A. Hourlier-Fargette, Y. Xue, H. U. Chung, and J. Y. Lee, "Relation between blood pressure and pulse wave velocity for human arteries," *Proc. Nat. Acad. Sci. USA*, vol. 115, no. 44, pp. 11144–11149, 2018, doi: 10.1073/pnas.1814392115.

[6] S. G. Yazdi, P. H. Geoghegan, P. D. Docherty, M. Jermy, and A. Khanafer, "A review of arterial phantom fabrication methods for flow measurement using PIV techniques," *Ann. Biomed. Eng.*, vol. 46, no. 11, pp. 1697–1721, Nov. 2018, doi: 10.1007/s10439-018-2085-8.

[7] F. S. Solberg, S. Kohtala, H. Vestad, and M. Steinert, "A combined photoplethysmography and force sensor prototype for improved pulse waveform analysis," in *Proc. IEEE SENSORS*, Oct. 2019, pp. 1–4, doi: 10.1109/SENSORS43011.2019.8956487.

[8] M. Kaisti *et al.*, "Clinical assessment of a non-invasive wearable MEMS pressure sensor array for monitoring of arterial pulse waveform, heart rate and detection of atrial fibrillation," *NPJ Digit. Med.*, vol. 2, no. 1, May 2019, doi: 10.1038/s41746-019-0117-x.

[9] S. Chen, J. Qi, S. Fan, Z. Qiao, J. C. Yeo, and C. T. Lim, "Flexible wearable sensors for cardiovascular health monitoring," *Adv. Healthcare Mater.*, vol. 10, no. 17, Sep. 2021, Art. no. 2100116, doi: 10.1002/adhm.202100116.

[10] G. Jo, T.-H. Yang, J.-H. Koo, M.-H. Jun, and Y.-M. Kim, "A transfer function model development for reconstructing radial pulse pressure waveforms using non-invasively measured pulses by a robotic tonometry system," *Sensors*, vol. 21, no. 20, p. 6837, Oct. 2021, doi: 10.3390/s21206837.

[11] W. Felt, K. Y. Chin, and C. D. Remy, "Contraction sensing with smart braid McKibben muscles," *IEEE/ASME Trans. Mechatronics*, vol. 21, no. 3, pp. 1201–1209, Jun. 2016, doi: 10.1109/TMECH.2015.2493782.

[12] W. Felt and C. D. Remy, "Smart braid: Air muscles that measure force and displacement," in *Proc. IEEE/RSJ Int. Conf. Intell. Robots Syst.*, Sep. 2014, pp. 2821–2826, doi: 10.1109/IROS.2014.6942949.

[13] A. V. Prituja, H. Banerjee, and H. Ren, "Electromagnetically enhanced soft and flexible bend sensor: A quantitative analysis with different cores," *IEEE Sensors J.*, vol. 18, no. 9, pp. 3580–3589, May 2018, doi: 10.1109/JSEN.2018.2817211.

[14] W. Felt and C. David Remy, "A closed-form kinematic model for fiber-reinforced elastomeric enclosures," *J. Mech. Robot.*, vol. 10, no. 1, Nov. 2017, doi: 10.1115/1.4038220.

[15] J. Vaicekauskaite, P. Mazurek, S. Vudayagiri, and A. L. Skov, "Mapping the mechanical and electrical properties of commercial silicone elastomer formulations for stretchable transducers," *J. Mater. Chem. C*, vol. 8, no. 4, pp. 1273–1279, Jan. 2020, doi: 10.1039/C9TC05072H.

[16] T. Ha, J. Ma, J. Blindheim, T. Welo, G. Ringen, and J. Wang, "In-line springback measurement for tube bending using a laser system," *Proc. Manuf.*, vol. 47, pp. 766–773, 2020, doi: 10.1016/j.promfg.2020.04.233.

[17] H. V. Riekkinen, K. O. Karkola, and A. Kankainen, "The radial artery is larger than the ulnar," *Ann. Thoracic Surgery*, vol. 75, no. 3, pp. 882–884, Mar. 2003, doi: 10.1016/S0003-4975(02)04557-5.

[18] B. D. Cullity and C. D. Graham, *Introduction to Magnetic Materials*, 2nd ed. New York, NY, USA: Wiley, 2009.

[19] M. K. Feldman, S. Katyal, and M. S. Blackwood, "U.S. artifacts," *Radio Graph.*, vol. 29, no. 4, pp. 1179–1189, Jul. 2009, doi: 10.1148/rg.294085199.

[20] A. Cafarelli, P. Miloro, A. Verbeni, M. Carbone, and A. Menciassi, "Speed of sound in rubber-based materials for ultrasonic phantoms," *J. Ultrasound*, vol. 19, no. 4, pp. 251–256, Apr. 2016, doi: 10.1007/s40477-016-0204-7.

[21] C. Oberhauser, *Optimizing L Measurement Resolution for the LDC161x and LDC1101*. Dallas, TX, USA: Texas Instruments, Feb. 2016.

[22] *Sensor Design for Inductive Sensing Applications Using LDC. Rev C*. Texas Instruments, Dallas, TX, USA, May 2021.

[23] R. Monfaredi, "Robot-assisted ultrasound imaging: Overview and development of a parallel telerobotic system," *Minimally Invasive Therapy Allied Technol.*, vol. 24, no. 1, pp. 54–62, 2015, doi: 10.3109/13645706.2014.992908.

Torjus L. Steffensen was born in Bergen, Norway, in 1993. He received the M.Sc. degree in mechanical engineering from the Norwegian University of Science and Technology (NTNU) in 2019, where he is currently pursuing the Ph.D. degree in medical technology with the TrollLABS.

His research interests include soft sensors, wearable longitudinal health monitoring, and data processing methods for physiology time series data.

Marius Auflem was born in Stavanger, Norway, in 1992. He received the M.Sc. degree in mechanical engineering from the Norwegian University of Science of Technology (NTNU) in 2018.

He currently works as an Industrial Ph.D. candidate at the TrollLABS, NTNU, together with Laerdal Medical. His research interests include medical simulation technology, soft robotics, and prototyping in the early stages of product development.

Håvard N. Vestad (Member, IEEE) was born in Bergen, Norway, in 1993. He received the M.Sc. degree in mechanical engineering from the Norwegian University of Science and Technology in 2018, where he is currently pursuing the Ph.D. degree with the Prototyping Laboratory TrollLABS.

His research interests include soft robotics and sensors, prototyping methodology, and early prototyping concept development for complex sensor problems.

Martin Steinert was born in Dresden, Germany. He received the B.A., M.A., and Ph.D. (Dr.Rer.Pol) degrees from the University of Fribourg, Switzerland, majoring in technology management.

He has been an Assistant Professor at the University of Fribourg, Switzerland, and a Visiting Scholar at the MIT and Stanford University before changing full-time to Stanford University as the Deputy Director of the Center for Design Research (CDR), and an Assistant Professor (Acting) of Mechanical Engineering with Stanford University. Since 2013, he has been a Full Professor of Engineering Design at the Department of Mechanical and Industrial Engineering (MTP), Norwegian University of Science and Technology (NTNU). He is a Professor of the NTNU. As of August 2021, he has more than 200 publications. His research interests focus on the fuzzy front end of new product development and design: optimizing the intersection of engineering design thinking and new product development, mechatronics/sensors, and computer sciences (especially machine learning). A special focus is on conceptual development and alpha prototype generation of high-performance requirements, as well as on experimental tools and setups.

Dr. Steinert has been a member of the Norwegian Academy of Technological Sciences (NTVA) since 2015. He has several prizes in both teaching and research.